Analytical Methods

Accepted Manuscript

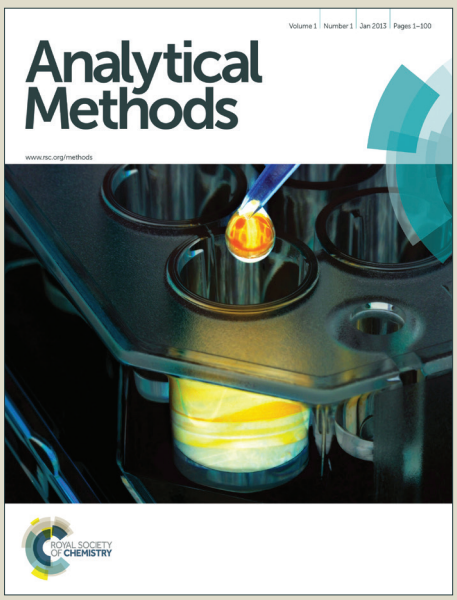

ROYAL SOCIETY OF CHEMISTRY

www.rsc.org/methods

RESEARCH ON THE DETECTION OF SF_6 DECOMPOSITION PRODUCTS BASED ON NON-RESONANT PHOTOACOUSTIC SPECTROSCOPY

J. Luo, Y. H. Fang*, Y. D. Zhao, A. J. Wang, D. C. Li, Y. Y. Li, Y. Liu, F. X. Cui, J. Wu, J. X. Liu

Key Laboratory of Optical Calibration and Characterization, Anhui Institute of Optics and Fine Mechanics, Chinese Academy of Sciences, Hefei 230031, China

** Author to whom correspondence should be addressed. Email: yhfang@aiofm.ac.cn*

Abstract: Under the action of Partial Discharge (PD), Gas Insulated Switchgear (GIS) will produce SF_6 decomposition products. If the concentration of these products is higher than some normal value, it indicates that the GIS equipment is faulty. The photoacoustic spectroscopy techniques have high sensitivity and good stability and further more they can realize on-line monitoring, which make them widely used in detection of SF_6 decomposition products in GIS equipments. The basic principles of photoacoustic spectroscopy were introduced and a set of device for the online detection of SF_6 decomposition based on non-resonant photoacoustic was designed and realized. According to the Infrared spectral characteristics of the target gases, the appropriate narrow band filters and infrared radiation light source were selected. This detection system is able to detect CO, SO_2 and CF_4 currently. Calibration experiments of different concentrations of CO, SO_2 and CF_4 were carried out and the results show that photoacoustic signal and the concentration have a perfect linear relationship and the detection limit for CO, SO_2 and CF_4 are 5.9116ppm, 8.2824ppm and 5.5226ppm. Relative errors of single measurement of CO, SO_2 and CF_4 are all less than 10% and the system exhibits excellent stability in a 12-hour continuous measurement.

Keywords: photoacoustic spectroscopy; non-resonant; online; filters; detection limit

1 Introduction

Gas Insulated Switchgear (GIS) has many advantages such as: small footprint and high reliability, which makes it widely used in electric equipments [1]. However, the whole components are sealed by the metallic shell which makes it hard to discover the initial failures. So it is necessary to monitor the inside fault of the GIS through some techniques in order to avoid accidents.

Sulphur hexafluoride is almost non-reactive and therefore it is widely used for insulation and current interruption purpose in electric power transmission and distribution equipment. Normally SF_6 is hard to decompose, but under the action of Partial Discharge (PD) and superheat, it can be decomposed into SF_2, SF_4, SF_5 and S_2F_{10}. If SF_6 is pure, these components will regain quickly [2-6]. If not, they will react with trace O_2 and H_2O and generate SO_2, SOF_2, SO_2F_2, CO and CF_4 etc. Preliminary study indicates that under different PD insulating faults, the decomposition products of SF_6 will be different in types, contents, production rates and ratios. In that case, we can establish the relationship between SF_6 decomposition and PD and then determine the cause and the extent of the risk of PD.

At present, there are many methods to detect SF_6 decomposition such as gas chromatography, detector tube and infrared absorption spectroscopy [7, 8]. Although these methods have their own

advantages, none of them could realize online detection.

What photoacoustic spectroscopy detects is the absorption energy and because it doesn't need to be compared to the incident light intensity, it can get high sensitivity [9]. In recent years, photoacoustic spectroscopy technology has been widely used in the power industry. Since 2000, photoacoustic spectroscopy has been successfully applied to develop Transfix oil dissolved gas analyzer, which can detect 8 kinds of fault gases in transformer oil and moisture content, by British Kelman Company [10]. State Key Laboratory of Power Transmission Equipment & System Security and New Technology of Chongqing University in China, which are led by Professor Tang, successfully developed a detection device for exploded component of SF_6 based on resonance photoacoustic spectroscopy in 2011 [11]. The QC team of Zibo Power Company in Shandong province combined Co., Ltd of Huigong in China, successfully developed a photoacoustic spectroscopy detector for SF_6 decomposition products based on the resonant photoacoustic spectroscopy. For the key component of photoacoustic detector-photoacoustic cell, Chongqing University and Zibo Power Company both used the resonant structure. Compared to the complex resonant structure, non-resonant photoacoustic cell has a simple structure, small size, low cost, easy to implement instrumentation and so on. Furthermore, it could satisfy the required sensitivity for detection of failures in Gas Insulated Switchgear by and large, which was put forward by Singapore Power Company who had noted that when the concentration of SO_2 exceeds 8ppm, the device needs overhaul. So a set of on-line device based on non-resonant photoacoustic spectroscopy was designed and preliminary results show that the device has a high sensitivity and good stability.

2 The principles of Photoacoustic Spectroscopy

Gas molecules sealed in photoacoustic cell are excited to high energy levels after absorbing the modulated light at a specific wavelength, and then the excited molecules will subsequently relax to the ground state through emission of photons or in a non-radiative way. These processes produce heats which in turn result in periodic pressure fluctuation. With highly sensitive microphones, the pressure fluctuation can be detected and converted into electric signal [12-13]. For the quantitative relationship between the photoacoustic signal and the gas concentration, we could get the gas volume fraction by detecting the photoacoustic signal. The basic principles are shown in Fig. 1.

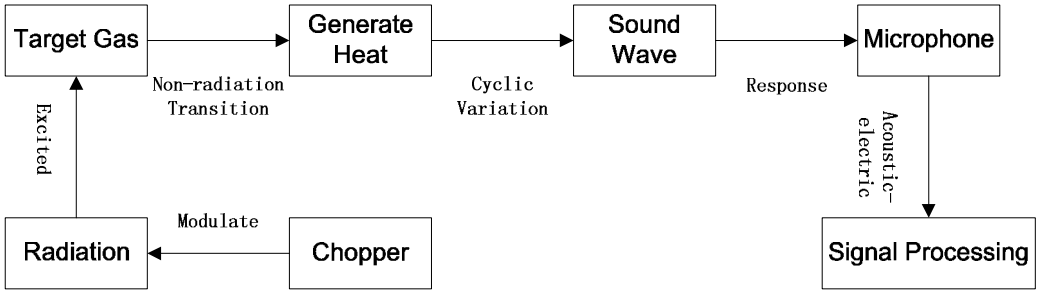

FIGURE 1 Schematic of photoacoustic detection principles

Heat generated by light absorption can be seen as the power density of a hot gas source:

$$\nabla^2 p - C_A^{-2} \frac{\partial^2 \mathrm{p}}{\partial \mathrm{t}^2} = -\left[\frac{(\gamma - 1)}{C_A^{\ 2}}\right] \frac{\partial H}{\partial t} \qquad (1)$$

Wherein C_A is the speed of sound in the gas, γ is the adiabatic exponent.

Eq. (1) is the non-homogeneous wave equation [14] and by solving it we can get the expression of amplitudes A_j:

$$A_{\mathrm{j}} = -\frac{i\omega}{{\omega_j}^2} \cdot \frac{\alpha[(\gamma-1)/V_{\mathrm{C}}]\int p_j(\vec{r}) * I(\vec{r},\omega)dV}{(1-\omega^2/{\omega_j}^2 - i\omega/\omega_j Q_j)} \tag{2}$$

When the modulation frequency of the incident light is lower than the lowest-order resonance frequency of photoacoustic cell, the only non-zero mode is p_0, the resonance frequency ω_0 is 0, and this time photoacoustic cell works in a plane wave:

$$A_0(\omega) = \frac{i\alpha(\gamma-1)\int I(\vec{r},\omega)dV}{\omega V_C[1+(I/\omega\tau_T)]} \tag{3}$$

Where α is the absorption coefficient of the gas, V_C is the volume of the photoacoustic cell, ω is the modulation frequency andτ_T is the thermal damping time.

Non-resonant photoacoustic cell is used in this paper, so the amplitude of the photoacoustic signal can be expressed as Eq. (3). The photoacoustic voltage signal after conversion from microphone can be expressed as:

$$U = S_{\min} \cdot P_s \cdot C_{cell} \cdot N \cdot \sigma \tag{4}$$

Where S_{min} is the microphone sensitivity (mV / Pa), P_s is the source power (W), C_{cell} is the photoacoustic cell constant (Pa · cm / W), which generally relates to the photoacoustic cell geometry and the physical constants of carrier gas, etc. N is the total number of molecule per unit volume (mol/cm^3), σ is the absorption cross section of the gas (cm^2).

As is seen in Eq. (4), when the other parameters remain unchanged, there is a good linear relationship between the photoacoustic signal and the gas concentration, so by calibrating the relationship equation between the photoacoustic signal and the concentration of the test gas, the concentration of target gas can be calculated.

3 Basic Composition

Our non-resonant photoacoustic detection device is shown in Fig. 2.

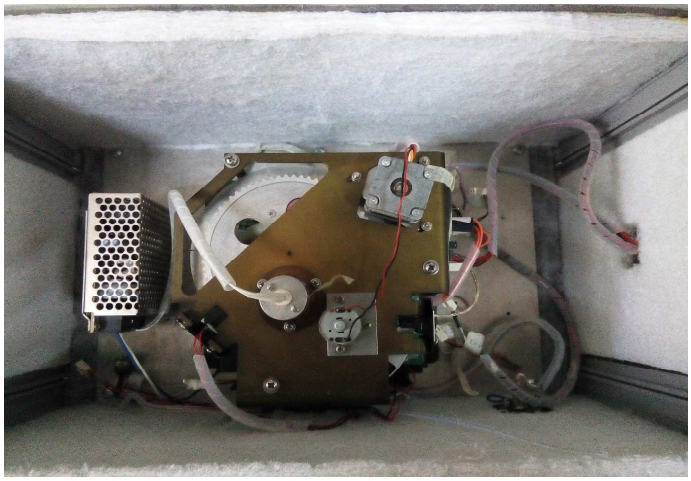

FIGURE 2 Photo of non-resonant photoacoustic detection device

The detector device consists of a light source, a chopper, filters, photoacoustic cell, a microphone, a control module which controls the rotation of the chopper plate and disc filter, and data acquisition and processing modules. The light passed through the filter after chopping into the photoacoustic cell, then a data acquisition module collected photoacoustic signal and sent it into the data processing module for processing, and finally through further analysis the type and concentration of the gas were obtained.

3.1 The Selection of Light Source and Filters

For most micro molecular gases, the vibration absorption bands are in the near and middle infrared regions, which are called "fingerprint region". The radiation source suitable for this wavelength range can be divided into coherent and non-coherent light source in accordance with the luminescence mechanism. Coherent light source with a large radiation power density and good monochromaticity usually can only achieve line tuning or continuous tuning within a very narrow range. There are limitations in the detection of gas species. The non-coherent source, based on the principle of the infrared radiation, generally has an approximate continuous spectral distribution of the blackbody radiation. Moreover such light source is low-cost and has a broad emission spectrum which makes it convenient to be used combining with narrow-band filters. But the power density of such a light source is low and not conducive to improve the sensitivity of photoacoustic detection. The IR-19-type broadband infrared light source is selected, and in order to improve the utilization efficiency of the light source, the ellipsoidal reflector with better convergence is used and plated. The broadband infrared radiation source is used in conjunction with various narrowband filters to get narrowband infrared light, which could stimulate specific test gas to generate photoacoustic signal. The operating state of IR-19 infrared light source is shown in Fig. 3 and the impression drawing of IR-19 infrared light source coordinated with ellipsoidal reflector is shown in Fig. 4.

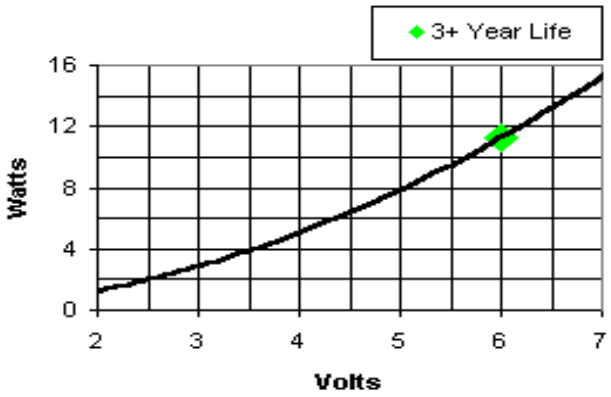

FIGURE 3 The operating state of IR-19 infrared light source

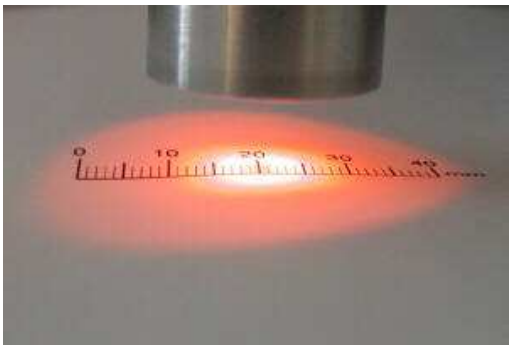

FIGURE 4 Schematic of effect of IR-19 light source coordinated with ellipsoidal mirror

As can be seen from Eq. (4), the photoacoustic signal U is proportional to the light power Ps and the absorption cross section σ of the gas to be measured. So the narrowband filters with suitable center wavelength and bandwidth are chosen to enhance the absorption cross-section of the tested gas and the optical power incident into the photoacoustic cell to a certain extent. In addition, cross interference from other potential interfering species has to be avoided as far as possible. In the present system CO, SO_2, and CF_4 are the main objects to be detected and the main interference gases are SF_6, CO_2 and H_2O. Fig.5 is a spectrogram of standard infrared absorption cross section of five gases, which was calculated by line-by-line integration method combined with HITRAN2004 database at the standard state [15].

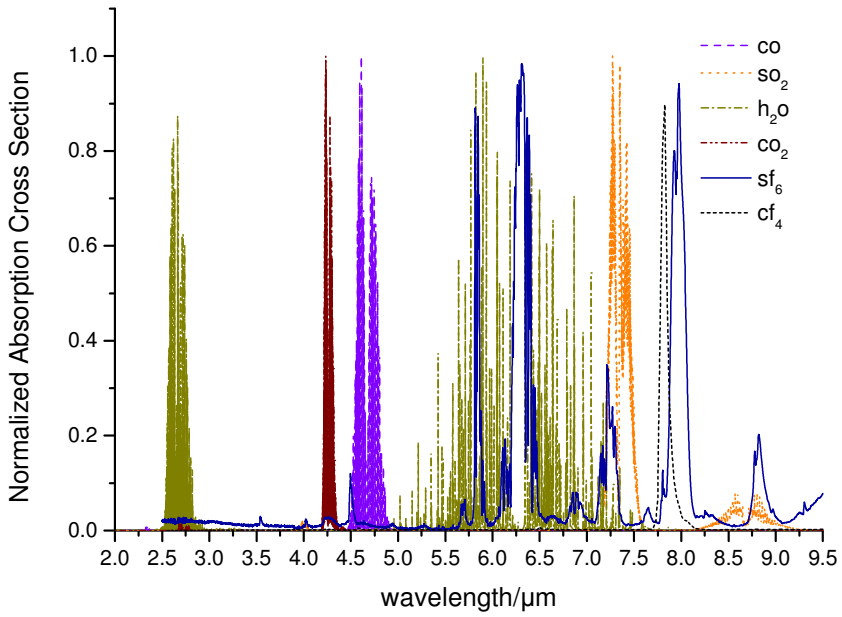

FIGURE 5 Spectrogram of standard infrared absorption cross section of CO、SO_2、H_2O、CO_2、SF_6 and CF_4

The characteristic absorption peaks of CO, SO_2, and CF_4 gases can be selected by comparing the absorption peaks shown in Fig. 5. For the selection of filters, we should not only ensure adequate gas absorption intensity, but also avoid severe cross interference with other gases, besides we should choose the short-wave direction as close as possible to ensure that the light intensity through the filter is not too weak. According to the principles, we have selected the filters of CO, SO_2 and CF_4, the spectral transmittances of which are shown in Fig. 6, Fig. 7 and Fig. 8, and the specific parameters of the selected filters are shown in Tab. 1.

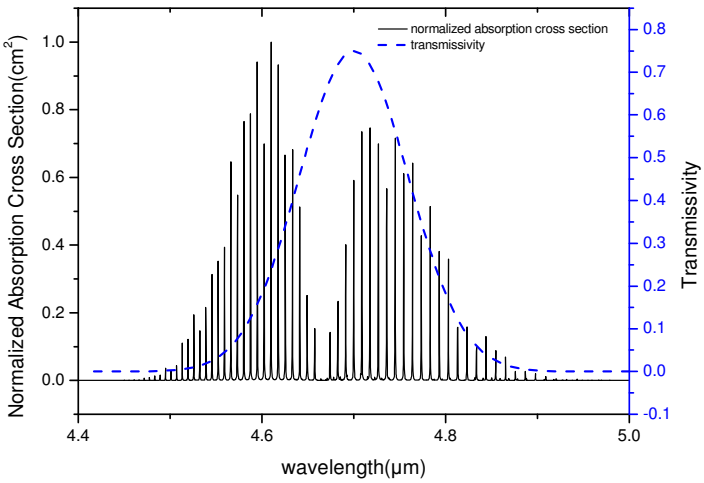

FIGURE 6 Diagram of transmissivity of carbon monoxide

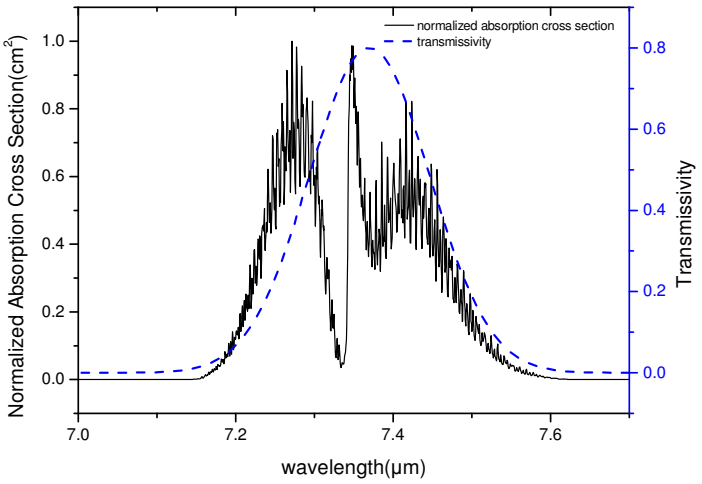

FIGURE 7 Diagram of transmissivity of sulfur dioxide

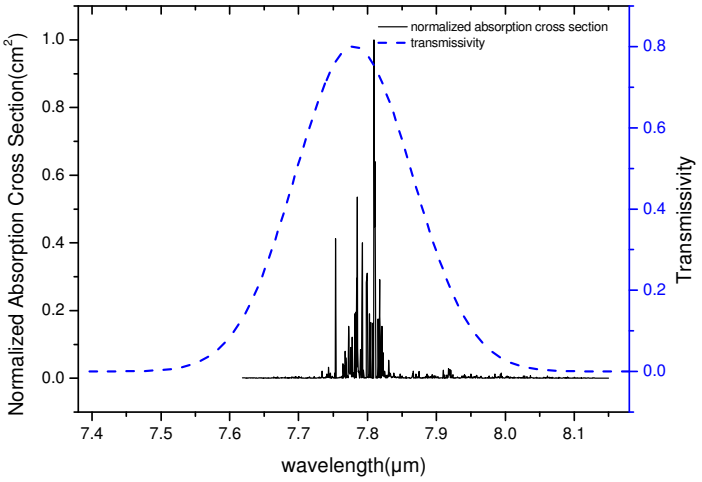

FIGURE 8 Diagram of transmissivity of carbon tetrafluoride

Table 1 Specific parameters of selected filters

Filters	CWL(μm)	HPB(nm)	Transmissivity (%)
CO	4.70	140	75
SO_2	7.37	180	80
CF_4	7.78	200	80

3.2 The Design of Photoacoustic Cell

Photoacoustic cell is a place where gas absorbs modulated light and photoacoustic effect happens

and also it is the key factor that influents photoacoustic spectrometer detection sensitivity. Based on different operation modes, photoacoustic cell can be divided into resonant and non- resonant cell [16]. When the modulation frequency of the incident light is much lower than the lowest-order resonance frequency, the photoacoustic cell operates in a non-resonant mode. The inner pressure of photoacoustic cell equals almost everywhere and changes with the modulation frequency of the incident light goes by.

For non-resonant photoacoustic cell, as mentioned previously, the only non-zero mode in photoacoustic cell was p_0 and its mode amplitude can be expressed as Eq. (3).If the total power of the light incident is represented by P_s, then Eq. (3) can be rewritten as Eq. (5):

$$A_0(\omega) = \frac{i\alpha(\gamma-1)P_s}{\omega V_C[1+(I/\omega\tau_T)]} \quad (5)$$

As is seen in Eq. (5), several aspects [17] as follows could be taken into consideration, which could improve the signal-to-noise ratio (*SNR*) of the non-resonant photoacoustic signal:

a) Increase the luminous power ripped into acoustic cell. Besides the increase of the radiation intensity of the source, multiple reflections can be applied to amplify the effective optical power;

b) Reduce the modulation frequency of the light source appropriately. Of course, the modulation frequency is not as small as possible , when the modulation frequency is very low, the responsive ability of microphone becomes weak;

c) Gas with relatively larger adiabatic index should be chosen as carrier gas, but for the detection of decomposition products of SF_6 in GIS, the carrier gas can only be sulphur hexafluoride;

d) Reduce the cross-sectional area of photoacoustic cell appropriately, but the coupling of the incident light and the microphone installation must be taken into account.

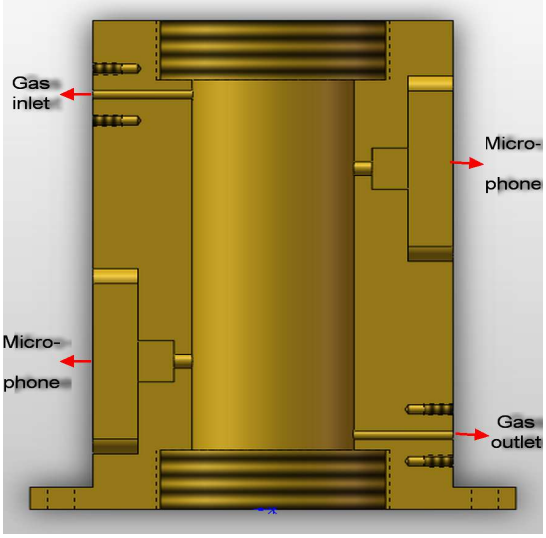

FIGURE 9 Profile schematic of non-acoustic cell

Fig. 9 is a profile schematic of photoacoustic cell designed by our team. The photoacoustic cell has a simple structure and small size. Furthermore, it is easy to realize instrumentation and its sensitivity can reach ppm.

4 Calibration of SF_6 Decomposition Components

The measurement was performed initially using a 499ppm mixture of carbon monoxide in SF_6 into

the photoacoustic cell at normal temperature-pressure (NTP) [18-20]. Small concentrations of the gas were synthesized by using electronic mass-flow controller. The electronic mass-flow controller was connected in parallel to the gas inlet of the photoacoustic cell and the initial CO concentration of 499ppm was diluted with pure SF_6 (zero gas) down to the lower concentrations. The standards CO of lower concentrations were filled in the photoacoustic cell the process of which lasted two minutes and the experiment under different filters began. The linear relationship between photoacoustic signal and the concentration of carbon monoxide using least squares fitting algorithm is shown in Fig. 10 and Eq. (6):

$$u\_co = 0.00181 \cdot c\_co + 2.51719 \quad (6)$$

Where *u_co* is the PA signal of CO and *c_co* is the concentration of CO.

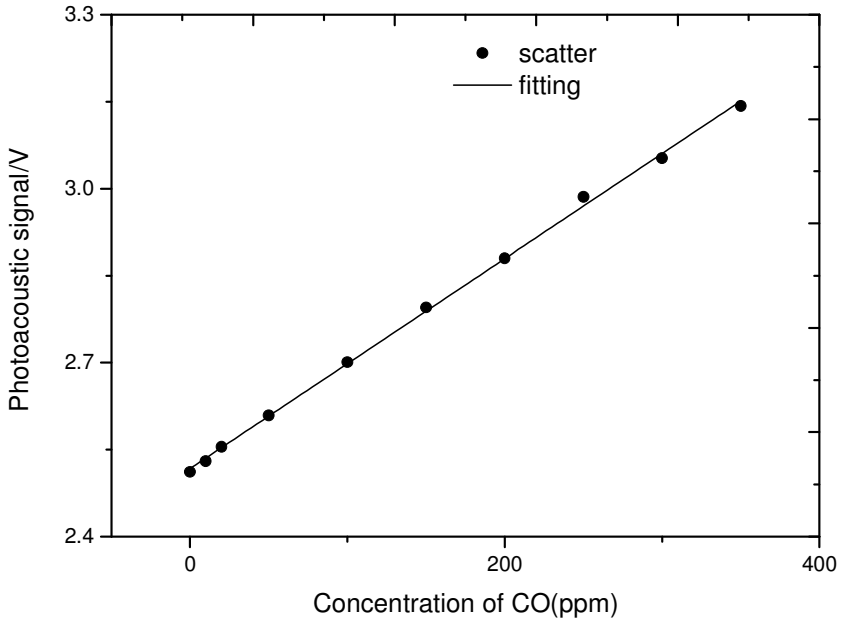

FIGURE 10 Schematic of relationship between concentration and photoacoustic signal of CO

The initial concentration of 400 ppm of sulfur dioxide was diluted with pure sulphur hexafluoride down to a series of lower concentrations using a mass-flow controller maintaining the same experimental conditions as was in the measurement experiment of carbon monoxide. The standard gases were filled in the photoacoustic cell successively and two minutes later, the measurement of photoacoustic signal of sulfur dioxide gas under different filters began. The linear relationship between photoacoustic signal and the concentration of sulfur dioxide using least squares fitting algorithm is gained, as is shown in Fig. 11 and Eq. (7). The same experimental procedure can also be applied to the measurement of CF_4 and the results are shown in Eq. (8) and Fig. 12. It should be noted that after every measurement the photoacoustic cell and gas circuit must be flushed using purity sulphur hexafluoride to avoid cross interference.

$$u\_so_2 = 0.0002314 \cdot c\_so_2 + 1.63222 \quad (7)$$

$$u\_cf_4 = 0.00019182 \cdot c\_cf_4 + 0.742722 \quad (8)$$

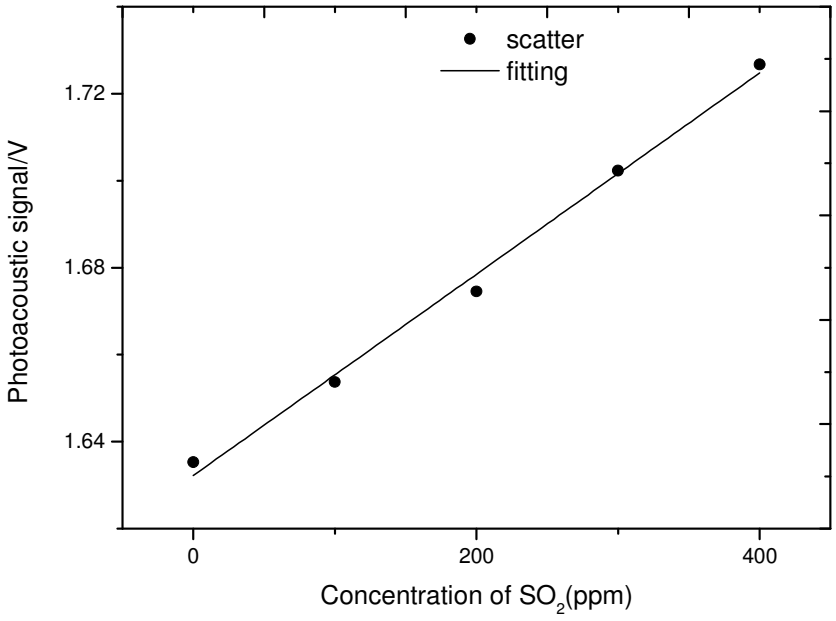

FIGURE 11 Schematic of relationship between concentration and photoacoustic signal of SO_2

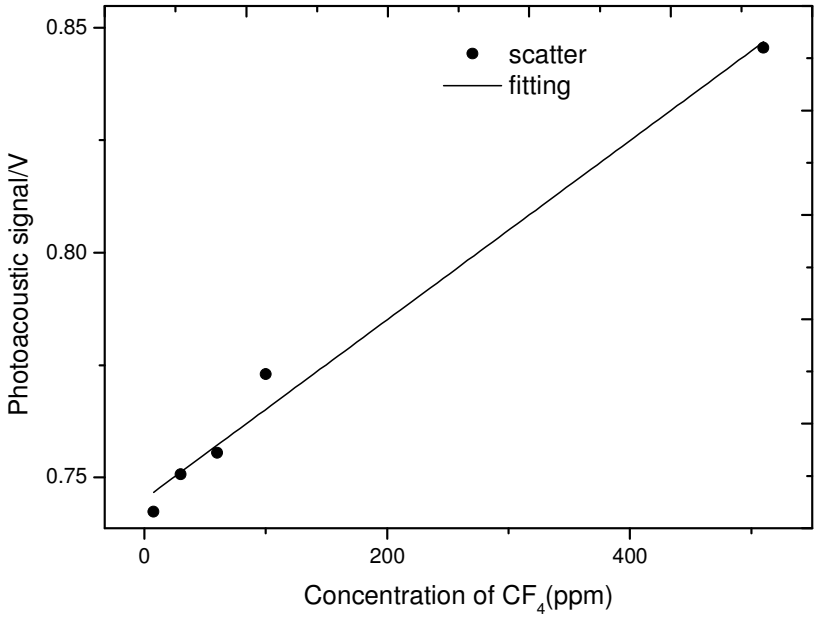

FIGURE 12 Schematic of relationship between concentration and photoacoustic signal of CF_4

As is shown in Fig. 10, Fig. 11 and Fig. 12, there is a good linear relationship between the photoacoustic signal and gas concentration, and the goodness of fit all reach 0.99 or more, which

verified the previous theory, in addition you can also see the fitting line does not pass through the original point, which is caused by the background noise.

5 Performance of The System

5.1 Detection Limit

The minimum detection limit is the concentration that can be detected when the signal to noise ratio (SNR) is equal to 1, which is mainly affected by systematic noise. There are many kinds of systematic noises, such as chopper noise, absorbing noise of cell walls and windows, circuit noise, air turbulence noise and environmental noise [21]. To determine the detection limit of the system, a dilution of a standard mixture of 132ppm of CO in SF_6 was filled in the photoacoustic (PA) cell and the measurement of photoacoustic signal under different filters began after two minutes at normal temperature-pressure (NTP). In order to improve the measurement precision, the gross errors of measuring results were removed using Grubbs criterion and the testing values of repeated measurements were averaged [22]. Here the standard deviation was regarded as the estimated value of the systematic noise. According to Eq. (9), the detection limit of CO is obtained. Similarly, the detection limit of SO_2 and CF_4 are calculated as shown in Tab. 2.

$$c_{\min} = \frac{c}{SNR} \tag{9}$$

Where c_{min} is the detection sensitivity, c is the known concentration of target gas and SNR the signal to noise ratio.

Table 2 The background signals and systematic noise of different filters

Filters	CO	SO_2	CF_4
Systematic noise(V)	0.0107	0.0019	0.0011
Detection Limit(ppm)	5.9116	8.2824	5.5226

5.2 Accuracy Analysis

According to the above analysis, the concentrations of target gases can be calculated using the Eq. (6), (7) and (8). In order to verify the accuracy of the detection system, three different mixed gases composed of different concentrations of CO, SO_2, and CF_4 were prepared. Tab. 3 shows the comparison results determined by Gas Chromatography and Photoacoustic Spectrometry. Here the result detected by Gas Chromatography was regarded as the true value of the concentration, and then the relative error of the photoacoustic detection system is:

$$e = \frac{\left|C_{PAS} - C_{real}\right|}{C_{real}} \times 100\% \tag{10}$$

Where C_{PAS} is the detection results of photoacoustic spectrometer, C_{real} the detection results of Gas Chromatograph.

Table 3 Comparison of results determined by Gas Chromatography and Photoacoustic Spectrometry

Mixed Gases	Gas Chromatography			Photoacoustic Spectrometry					
	CO (ppm)	SO_2 (ppm)	CF_4 (ppm)	CO (ppm)	*e* (%)	SO_2 (ppm)	*e* (%)	CF_4 (ppm)	*e* (%)
1	132	145	510	133.5	1.1	141.8	2.2	508.4	0.3
2	63	80	30	65.8	4.4	83.2	4.0	31.8	6.0
3	27	37	7.5	28.7	6.3	40.3	8.9	6.8	9.3

As can be seen from Tab. 3, the detection errors of photoacoustic system for three target gases are all less than 10%, in which the deviation for CO is not more than 6.3% and for SO_2 and CF_4 not more than 8.9% and 9.3% respectively. The experimental results show that this detection system based on non-resonant photoacoustic spectroscopy is effective and could meet online testing requirements.

5.3 Stability Analysis

In order to realize real-time monitoring of SF_6 decomposition within GIS content, the detection system should have good stability [23-25]. Here the relative error *e* was used to evaluate the stability of the detection system again and the expression of *e* is shown in Eq. (9) above. Here C_{PAS} is the single measurement value of photoacoustic spectroscopy, and C_{real} is the actual value of the concentration.

Continuous measurements of the mixed gas composed of 13.6ppmCO, 32.2ppmSO_2 and 25.4ppm CF_4 were carried out. The whole experiment lasted 12 hours with the time interval of 1 hour. The measurement results are shown in Tab. 4 and Fig. 13.

Table 4 Experiments for the systematic stability

Measurement time(h)	CO(ppm)	Relative Error(%)	SO_2(ppm)	Relative Error(%)	CF_4(ppm)	Relative Error(%)
1	12.5	7.9	29.5	8.5	25.0	1.6
2	12.7	6.4	30.0	6.9	26.4	4.0
3	12.6	7.4	30.5	5.4	26.9	6.2
4	12.8	6.2	30.7	4.5	24.2	4.6
5	13.5	0.8	31.9	0.7	24.8	2.3
6	13.4	1.4	32.0	0.6	24.4	3.7
7	12.8	6.1	30.8	4.3	26.4	4.0
8	13.1	4.0	30.7	4.8	26.0	2.5
9	13.3	2.4	30.0	6.8	24.3	4.2
10	13.0	4.5	29.6	8.1	24.2	4.9
11	12.5	8.5	30.2	6.1	24.2	4.8

12	12.6	7.3	29.1	9.6	24.7	2.8

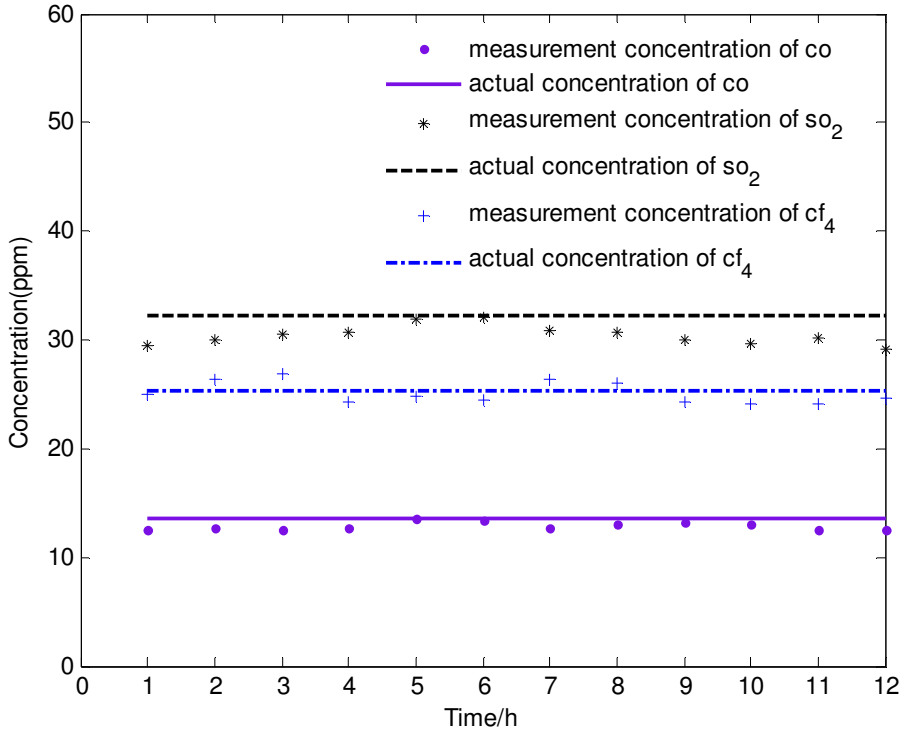

FIGURE 13 Concentrations of three target gases measured versus time

As can be seen from Tab. 5 and Fig. 13, with the continuation of the time, the detection concentrations of CO, SO_2 and CF_4 are basically in horizontal lines which take their respective actual concentrations as references. The relative errors of single measurement for CO, SO_2 and CF_4 are not more than 8.5%, 9.6% and 6.2% respectively. The PA system demonstrates good stability and could meet the online testing requirements for the detection of SF_6 decomposition products in GIS device.

6 Conclusion

The principle of photoacoustic spectroscopy was introduced and a set of system for the online detection of SF_6 decomposition in GIS based on non-resonant photoacoustic was designed and realized. According to the Infrared spectral characteristics of the target gases, the appropriate narrow band filters of three target gases and infrared radiation light source were selected. CO, SO_2 and CF_4 of the decomposition products were calibrated, and the performance of the system was tested. The results show that: (1) The minimum detection limits for CO, SO_2 and CF_4 have reached 5.9116ppm, 8.2824ppm and 5.5226ppm respectively; (2) Relative errors of single measurement are all less than 10%; (3) The photoacoustic system exhibits excellent stability in a 12-hour continuous measurement. Photoacoustic spectroscopy with higher sensitivity and good stability could realize online testing and has good prospects for development in the power industry.

Acknowledgements

This work was supported by Electric Power Research Institute of Anhui Province who provided the essential experimental materials, such as the calibrating gases and the electric mass-flow controller.

References

1. Y. S. Ji and C. Y. Wang, *High Voltage Apparatus*, 2011, **47**,100-107.
2. Q. Yao, Y. Wang and Y. Liu, *High Voltage Apparatus*, 2010, **46**, 53-59.
3. L. S. Luo and W. J. Yao, *Power System Technology*, 2010, **34**, 225-230.
4. Z. Zhou and S. Y. Chen, *High Voltage Apparatus*, 2011, **47**,104-107.
5. L. Y. Wan, Chong Qing University, 2008.
6. Z. Q. Guo, Shang Hai Jiao Tong University, 2008.
7. X. L. Yan and C. Y. Wang, *Power System Technology*, 2010, **34**, 160-165.
8. X. L. Yan and C. Y. Wang, *High Voltage Apparatus*, 2013, **49**, 1-9.
9. A. Elia, C. Di. France, P. M. Lugarà and G. Scamarcio, *Sensors*, 2006, **6**, 1411-1419.
10. C. Zhang and F. Wang, *High Voltage Engineering*, 2005, **31**, 84-86.
11. M. Fan, Chong Qing University, 2012.
12. A. Elia, P. Lugarà, C. Di. Franco and V. Spagnoto, *Sensors,* 2009, **9**, 9616-9628.
13. X. J. Peng, Chong Qing University, 2013.
14. H. Zhang and G. Y. Shi, *Chinese Journal of Atmospheric Sciences*, 2000, **24**, 112-121.
15. P. L. Meyer and M. W. Sigrist, *Rev.Sci.instrum*, **61**, 1779(1990); doi:10.1063/1.1141097.
16. A. Miklós, P. Hess and Z. Bozóki, *Rev.Sci.instrum*, **72**, 1937(2001); doi: 10.1063/1.1353198.
17. M. Tavakoli, A. Tavakoli, M. Taheri and H. Saghafifar, *Optics&Laser Technology*, 2010, **42**, 828-838.
18. H. Huszár, A. Pogány, Z. Bozóki, A. Mohácsi, L. Horvath and G. Szabo, *Sensors and Actuators B*, 2008, **134**, 1027-1033.
19. M. Szakáll, J. Csikós, Z. Bozóki and G. Szabó, *infrared physics&Technology*, 2007, **51**, 113-121.
20. V. Koskinen, J. Fonsen, J.Kauppinen and I. Kauppinen, *Vibrational Spectroscopy*, 2006, **42**, 239-242.
21. J.-p. Besson, S. Schilt and L. Thévenaz, *Spectrochimica Acta Part A*, 2006, **63**, 899-904.
22. Y. Zhao, Y. Pan, J. Rutherford and F. M. Mitloehner, *Atmosphere*, 2012, **3**, 246-265.
23. D. K. Havey, P. A. Bueno, K. A. Gillis, J. T. Hodges, G. W. Mulholland, R. D. V. Zee and M. R. Zachariah, *Anal. Chem*, 2010, **82**, 7935-7942.
24. M. W. Sigrist, *Infrared Phys. Technol*, 1995, **36**, 415-425.
25. E. D. McNaghten, K. A. Grant, A. M. Parkes and P. A. Martin, *Appl Phys B*, 2012, **107**, 861-871.